

# A ZIRCONIA COMPOSITE WITH THE IN-SITU SYNTHESIZED TITANIUM DIBORIDE INCLUSIONS

Waldemar Pyda, Norbert Moskała

AGH University of Science and Technology, Faculty of Materials Science and Ceramics, Al. Mickiewicza 30, 30-059 Cracow, Poland, [pyda@agh.edu.pl](mailto:pyda@agh.edu.pl),

**Keywords:** *composite powder, composites, TZP, TiB<sub>2</sub>, TiC, in-situ synthesis*

## Abstract

A composite in the TiO<sub>2</sub>-Y<sub>2</sub>O<sub>3</sub>-ZrO<sub>2</sub>/TiB<sub>2</sub> system was prepared by using the zirconia powder containing the in-situ synthesized TiB<sub>2</sub> inclusions. The reaction among carbon, boron oxide and titanium oxide dissolved in the 1.5 mol% Y<sub>2</sub>O<sub>3</sub>-18 mol% TiO<sub>2</sub>-ZrO<sub>2</sub> solid solution was utilized. Phenol-formaldehyde resin and H<sub>3</sub>BO<sub>3</sub> delivered carbon and boron to the reaction, respectively. The TiB<sub>2</sub> synthesis was performed for 4 h at 1500°C in vacuum. The resultant composite zirconia powder was characterised by XRD, TG/DTG and TEM/EDS methods. It contained mainly TiB<sub>2</sub> inclusions and small amount of TiC, ZrC and ZrB. The inclusions were of nearly nanometric in size. The powder was used to produce a zirconia matrix composite by means of hot pressing at 1500°C. The composite was characterised by XRD and SEM methods. It contained small amount of TiC beside the primary TiB<sub>2</sub> inclusions. A bending strength of 912±72 MPa and a fracture toughness of 8.8±0.5 MPa·m<sup>1/2</sup> were measured.

## 1 Introduction

Benefits of the transformation toughening and the presence of high hardness and rigid inclusions are utilized in the ceramic matrix composites of the tetragonal zirconia polycrystals stabilised with yttria (Y-TZP) and containing up to 50 % TiB<sub>2</sub> [1-3]. The increased fracture toughness comparing with titanium diboride and increased hardness comparing with Y-TZP have been found in these composites. Preparation of the composite powder with the appropriate particle size distribution and uniformity of the component particle dispersion is the first and crucial step of any composite technology. So far only a method of mechanical mixing of the zirconia and TiB<sub>2</sub> powders of the suitable particle size distribution has been used.

The aim of the presented work was to develop a new method of in-situ synthesis of the zirconia/TiB<sub>2</sub> composite powder and to evaluate its usability for production of the composites with improved mechanical properties. The method utilizes the reaction between titanium oxide dissolved in the zirconia solid solution and boron oxide in the presence of carbon serving as a reducing agent.

## 2 Experimental Procedure

A co-precipitation-calcination method was used to prepare the original zirconia powder stabilised with 1.5 mol% Y<sub>2</sub>O<sub>3</sub> and doped with 18 mol% TiO<sub>2</sub>. A water solution of ZrOCl<sub>2</sub> (>99%), YCl<sub>3</sub> (99.99%) and TiCl<sub>4</sub> (>98%) was treated with NH<sub>3(aq)</sub> (a.p.) at a pH of 9. The resultant zirconia hydrogel was washed with distilled water to remove NH<sub>4</sub>Cl, then dried at 110°C to a constant mass and calcined for 2 hrs at 700°C. A nanopowder of zirconia-yttria-titania solid solution with a crystallite size of ~20 nm and a specific surface area of 62.5±1.0 m<sup>2</sup>/g was obtained. The nanopowder contained 19.2±0.5 vol.% and 80.8±0.5 vol.% of the monoclinic and tetragonal zirconia polymorph, respectively.

A homogeneous mixture of the zirconia nanopowder, H<sub>3</sub>BO<sub>3</sub> (a. p.), and phenol-formaldehyde resin was prepared. A 20 wt% ethanol solution of the resin was used. A ratio of the components enabled titania, dissolved in the zirconia solid solution, to be fully reacted.

Homogenisation of the mixture was performed for 15 min. in isopropyl alcohol by using an attrition mill. The mixture was heat treated in four stages. The heating procedure was developed according to the DTA/TG analysis shown in Fig. 1. The dispersant was removed at 95°C in air during the drying stage. H<sub>3</sub>BO<sub>3</sub> was decomposed to give B<sub>2</sub>O<sub>3</sub> for the in situ synthesis during heating for 0.5 h at

300°C in argon. The phenol-formaldehyde resin was decomposed during heating for 1.5 hr at 800°C in argon. A heating rate of 20°C/min was used to achieve each soaking temperature. The resultant loose powder was inserted into a graphite crucible and then in a vacuum furnace chamber which was started to heat with a rate of 10°C/min up to 1500°C. The in-situ synthesis was performed for 4 hrs under a pressure of  $4.5 \cdot 10^{-7}$  atm. The as-synthesized composite powder was attrition milled for 6 hrs in isopropyl alcohol. Made from Y-TZP grinding media of 2 mm in diameter were used. The original and composite zirconia powders were hot pressed for 1 hr at 1500°C under 25 MPa in argon to obtain dense bodies.

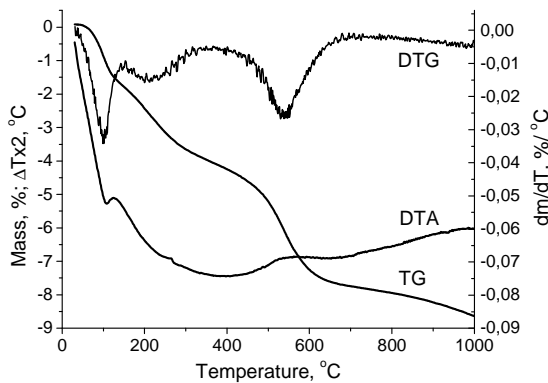


Fig. 1. DTA, TG and DTG patterns of the zirconia,  $H_3BO_3$ , and phenol-formaldehyde mixture heated at 10°C/min in argon. Ethanol and water evaporation, boric acid decomposition and resin decomposition are attributed to the overlapping effects of mass loss at 40-140°C, 140-370°C, 370-700°C, respectively.

The phase composition of the original and composite zirconia powder as well as the sintered bodies was determined by X-ray diffractometry. A  $CuK_{\alpha 1}$  radiation, an angular range of  $10-80^\circ 2\theta$  and a step of  $0,008^\circ 2\theta$  were used. The X'Pert Plus v1.0 software enabled Rietveld refinement of the diffraction patterns to be made [4]. Specific surface area of the powders was measured by nitrogen adsorption and the BET method. The powder morphology was observed using electron transmission microscopy (TEM). The EDS method was used to determine the chemical composition of the composite powder. The differential thermal analysis (DTA) and thermogravimetry (TG) were used to study a behaviour of the composite powder during heating at a rate of 10°C/min at a temperature range of 20-1000°C in air. It was done to show the presence of borides, carbides and unreacted carbon

in the studied system. An apparent density of the sintered bodies was measured by the Archimedes' method. Total porosity was assessed by using optical microscopy and a numerical image analysis method with the aid of the ImageJ 1.29x software [5]. An average value of the pore content was calculated from the measurements that were taken from three surface areas of the polished sample of  $430 \times 280 \mu m^2$  in size. Scanning electron microscopy coupled with the EDS technique was used to analyse the microstructure of the sintered samples. Vickers indentation was used to determine hardness and the critical stress intensity factor. A load of 1 kG and 30 kG was applied to the samples for 10 s, respectively. A Palmqvist crack model was applied for the  $K_{Ic}$  calculations [6]. Bending strength of the samples of  $2 \times 2.35 \times 21 mm^3$  was measured by the three point bending test using a span of 18 mm and a loading rate of 2 mm/min.

### 3 Results and Discussion

#### 3.1 Thermodynamic Fundamentals

In order to estimate a temperature at which the carbothermal reductions in the  $B_2O_3-TiO_2-ZrO_2$  system can take place, Gibbs free energies of the following reactions were calculated [7]:

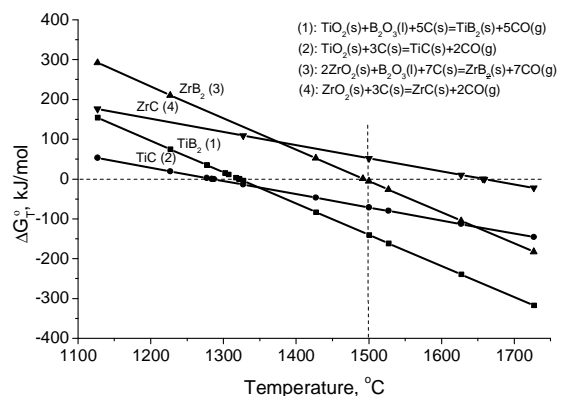
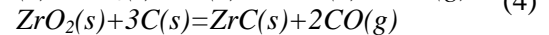
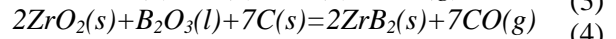
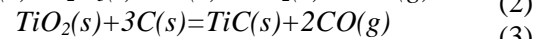
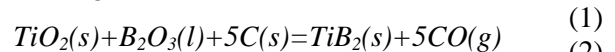


Fig. 2. Calculated standard Gibbs free energies as functions of temperature for the indicated reactions.

The data shown in Fig. 2 indicate that reactions (1) and (2) can occur ( $\Delta G_T^o = 0$ ) at about 1322°C and 1287°C, respectively, but the temperatures for the other two reactions to occur are much higher than the first two. This suggests an opportunity to react

TiO<sub>2</sub> with carbon and B<sub>2</sub>O<sub>3</sub> at a selected temperature while living ZrO<sub>2</sub> unchanged. Moreover, at a temperature of 1500°C selected for the in-situ experiment, the  $\Delta G_T^o$  value for TiB<sub>2</sub> formation is smaller (-140.3 kJ/mol) than for TiC (-71.3 kJ/mol) suggesting an opportunity to obtain the former phase primary.

### 3.2 Composite Powder

The method of in-situ synthesis delivered the zirconia powder which contained the tetragonal and monoclinic zirconia polymorph together with TiB<sub>2</sub>, TiC, ZrB and ZrC as shown in Fig. 3. The data of Table 1 confirm TiB<sub>2</sub> as the main in-situ synthesized phase. A TiB<sub>2</sub> content of 8.1±0.4 vol.% was measured. The results are consistent with the thermodynamic calculations in that point. The presence of ZrB and ZrC should be attributed to very low CO partial pressure of  $\sim 4.5 \cdot 10^{-7}$  atm during the in-situ synthesis. An increase of the monoclinic zirconia content, when compared to the original zirconia nanopowder, was detected as a result of zirconia crystallites growth accompanying the heat treatment applied. The values of 60.5±0.3 vol.% and 19.2±0.5 vol.% were measured for the heat treated and original zirconia nanopowder, respectively.

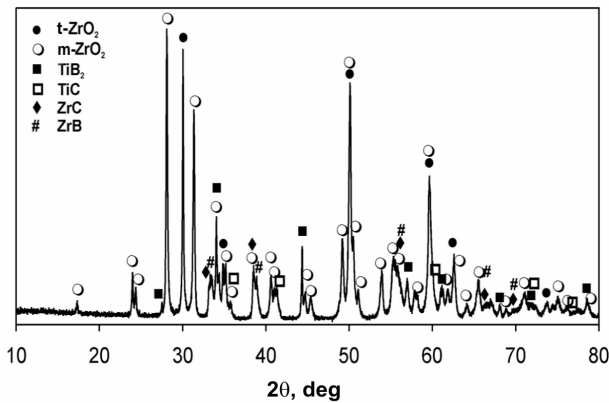


Fig. 3. X-ray diffraction pattern of the as-received composite powder; m and t – monoclinic and tetragonal zirconia, respectively

Table 1. Phase composition of the as-received composite powder

Tetragonal ZrO <sub>2</sub> , vol.%	Monoclinic ZrO <sub>2</sub> , vol.%	TiB <sub>2</sub> , vol. %	TiC, vol.%	ZrB, vol.%	ZrC, vol.%
19.6 ± 0.2	60.5 ± 0.3	8.1 ± 0.4	3.7 ± 0.3	4.1 ± 0.3	4.0 ± 0.2

The results of the DTA/TG analysis of the composite powder are shown in Fig. 4. The

presence of some amount of unreacted carbon is evidenced. A series of overlapping exothermic peaks, accompanied by an increase of the sample mass, appeared at the temperatures ranging from  $\sim 300^\circ\text{C}$  to  $762^\circ\text{C}$  when the sample was heat treated in air to  $1000^\circ\text{C}$ . It was attributed to the oxidation of borides and carbides as was confirmed by the X-ray measurements. After the DTA/TG analysis, the sample showed the presence of the monoclinic and tetragonal zirconia polymorph together with TiO<sub>2</sub> of the rutile symmetry. Simultaneously a distinct background elevation, which is characteristic of the amorphous phase, was observed as a result of the B<sub>2</sub>O<sub>3</sub> containing glassy phase presence. Broadening of the exothermic peak towards temperatures higher than the temperature of the sample mass increase cessation ( $730^\circ\text{C}$ ) originates from the unreacted carbon oxidation (Fig. 4).

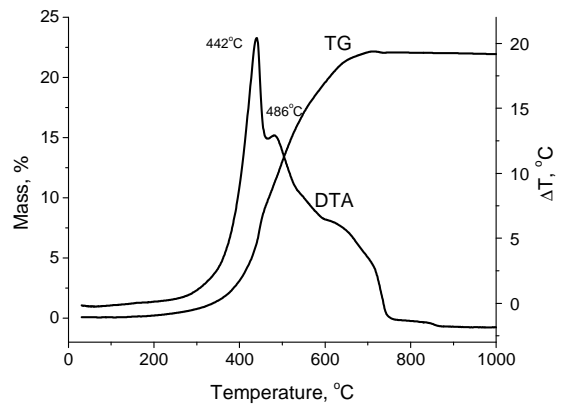


Fig. 4. TG and DTA curves of the composite powder heat treated in air with a heating rate of  $10^\circ\text{C}/\text{min}$

The composite powder received a specific surface area of  $16.6 \pm 0.5 \text{ m}^2/\text{g}$  due to the attrition milling applied. Its morphology is shown in Fig. 5. The powder was composed of isometric and needle-shaped crystallites of 250-500 nm in size. Comparison these particle sizes with the crystallite size of the original zirconia nanopowder gives evidence of intensive sintering of the composite mixture during the hard inclusion synthesis. This was accompanied by zirconia crystallite growth as suggested by a significant increase of the monoclinic zirconia content (Table 1).

The coupled TEM and EDS techniques were used to identify the phases existed. Maps of the zirconium, titanium and oxygen distribution within the agglomerate of Fig. 5 are shown in Fig. 6. The elongated particles were significantly enriched with titanium and devoid of zirconium and oxygen. This

suggests the  $\text{TiB}_2$  or  $\text{TiC}$  particles. Further recognition between these particles was not possible due to the lack of boron and carbon distribution maps.

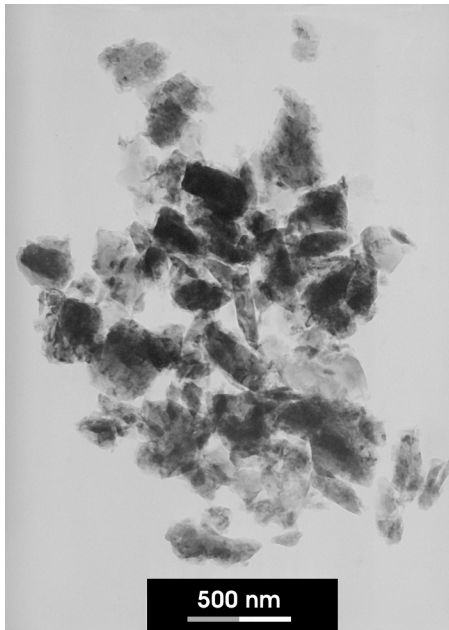


Fig. 5. TEM microphotograph of the composite powder after 6 h of attrition milling

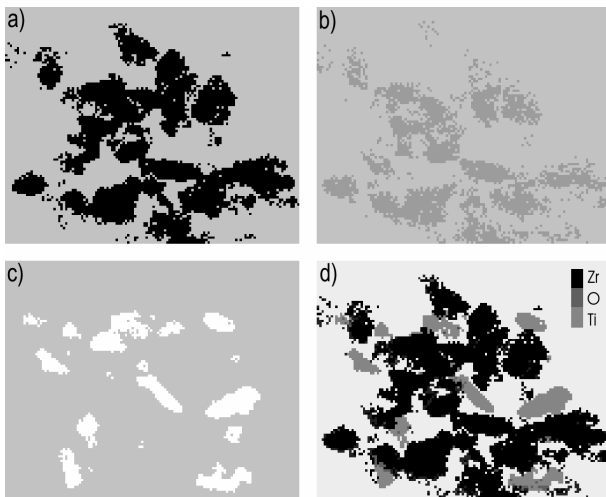


Fig. 6. Maps of the elements in the powder particles shown in Fig. 5 derived from the EDS analysis: a) zirconium, b) oxygen, c) titanium, d) setting-up of the Zr, Ti and O maps

The composite zirconia micropowder containing submicron hard particles was produced by the technique studied. The zirconia particle size was actually dependent on conditions of the attrition milling. However, the hard inclusion size and morphology were mainly affected by conditions of both the composite mixture preparation and the in-

situ synthesis. Uniform distribution of the substrates favoured crystallisation of the particles submicron in size. The zirconia nanocrystallites and the method of dispersion of carbon and boron precursors in liquid were used to this end. An additional factor being conducive to the hard inclusion formation was a behaviour of titanium in the zirconia lattice. Titanium ions substitute zirconium ions in the zirconia lattice showing a concentration gradient in the vicinity of free surfaces and grain boundaries. Allemann et al. [8] reported that the  $\text{Ti}^{4+}$  cation concentration in the grain boundary surface area is five times larger than in the grain interior of the  $\text{TiO}_2\text{-ZrO}_2$  solid solution. Therefore, titanium availability for the reaction with  $\text{B}_2\text{O}_3$  and C is increased. In addition, the segregation zone can show a significant size of  $\sim 6$  nm. Such zone can occupy significant part of the zirconia crystallite in case of the nanometric zirconia powder used in the study.

### 3.3 Sintered Materials

The X-ray diffraction measurements revealed the presence of  $\text{TiB}_2$  and  $\text{TiC}$  in the zirconia solid solution matrix of the tetragonal and monoclinic symmetry as shown in Fig. 7. Neither  $\text{ZrB}$  nor  $\text{ZrC}$  was detected. This result proves decomposition of the  $\text{ZrB}$  and  $\text{ZrC}$  inclusions during sintering and most probably explains an increased content of  $\text{TiB}_2$  and  $\text{TiC}$  in the composite material comparing to the composite powder (see Table 1 and 2). Assuming the completed reaction between  $\text{TiO}_2$  dissolved in the zirconia solid solution and carbon or additionally boron introduced to the system, the amount of 15 vol.%  $\text{TiB}_2$  and 12 vol.%  $\text{TiC}$  is calculated according to the reaction (1) and (2), respectively. A significant difference between the measured and calculated component phase balance suggests that nonstoichiometric  $\text{TiB}_2$  and  $\text{TiC}$  crystallized during the in-situ synthesis. This is consistent with the data reported in a prior work on the  $\text{TiC}$  in-situ crystallization [9].

The data of Tables 1 and 2 indicate an increase of the tetragonal zirconia content in the sintered composite when compared to the composite powder. This tendency is profitable because contribution of the transformation toughening to mechanical property improvement increases with the tetragonal phase content increase [10].

Table 2 contains also the results concerning the material derived from the original zirconia powder. It is called the original TZP due to similarities to the tetragonal zirconia polycrystals (TZP). The

composite material showed a decrease of the tetragonal phase content when compared to the original TZP sample. This can be attributed to a change of the chemical composition of the zirconia solid solution due to the in-situ  $\text{TiB}_2$  and  $\text{TiC}$  crystallization. A critical size of the zirconia grains can be affected by that chemical change [11].

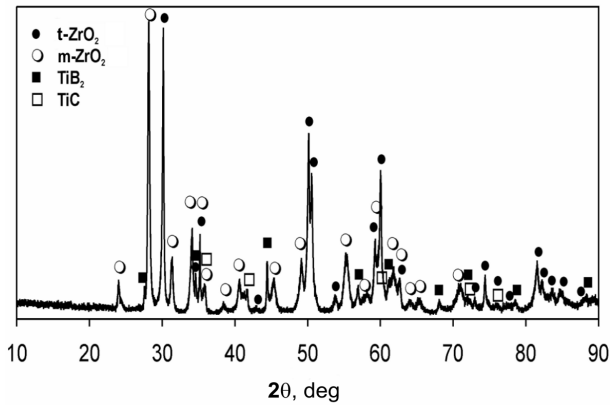


Fig.7. X-ray diffraction pattern of the composite hot-pressed for 1 h at 1500°C

Table 2. Phase composition of the composite and zirconia matrix hot-pressed at 1500°C

Material	Tetragonal $\text{ZrO}_2$ , vol.%	Monoclinic $\text{ZrO}_2$ , vol.%	$\text{TiB}_2$ vol.%	$\text{TiC}$ vol.%
Composite	32.1 $\pm 0.3$	47.2 $\pm 0.4$	12.9 $\pm 0.2$	7.8 $\pm 0.5$
Original TZP	67.3 $\pm 0.3$	32.7 $\pm 0.5$	-	-

Table 3. Selected properties of the composite and original TZP hot-pressed at 1500°C

Material	Relative density, $\text{g/cm}^3$	Total porosity, %	Bending strength, MPa	$K_{IC}$ , $\text{MPa m}^{0.5}$	HV, GPa
Composite	5.76 $\pm 0.01$	1.7 $\pm 0.3$	912 $\pm 72$	8.8 $\pm 0.5$	12.2 $\pm 0.2$
Original TZP	5.72 $\pm 0.01$	0.5 $\pm 0.4$	319 $\pm 75$	4.5 $\pm 0.2$	11.1 $\pm 0.2$

Densification of the composite powder was constrained by the in-situ inclusions as shown in Table 3. The composite material showed an apparent density of  $5.76 \pm 0.01 \text{ g/cm}^3$  and a total porosity of  $1.7 \pm 0.3\%$ . The TZP material made from the original zirconia powder reached porosity by 1.2% smaller than the composite. Inhibited grain growth was simultaneously observed in the composite as shown in Fig. 8. The resultant microstructure was more uniform and finer than the original TZP material microstructure. The latter one contained two grain populations of  $\sim 10 \mu\text{m}$  and  $\sim 2 \mu\text{m}$  in size,

respectively (Fig. 8c). In case of the composite microstructure, a mean size of the zirconia grains ranged from  $0.5 \mu\text{m}$  to  $1 \mu\text{m}$  (Fig. 8 b). A mean size of the titanium boride and carbide inclusions was comparable to the zirconia grain size (Fig. 8a).

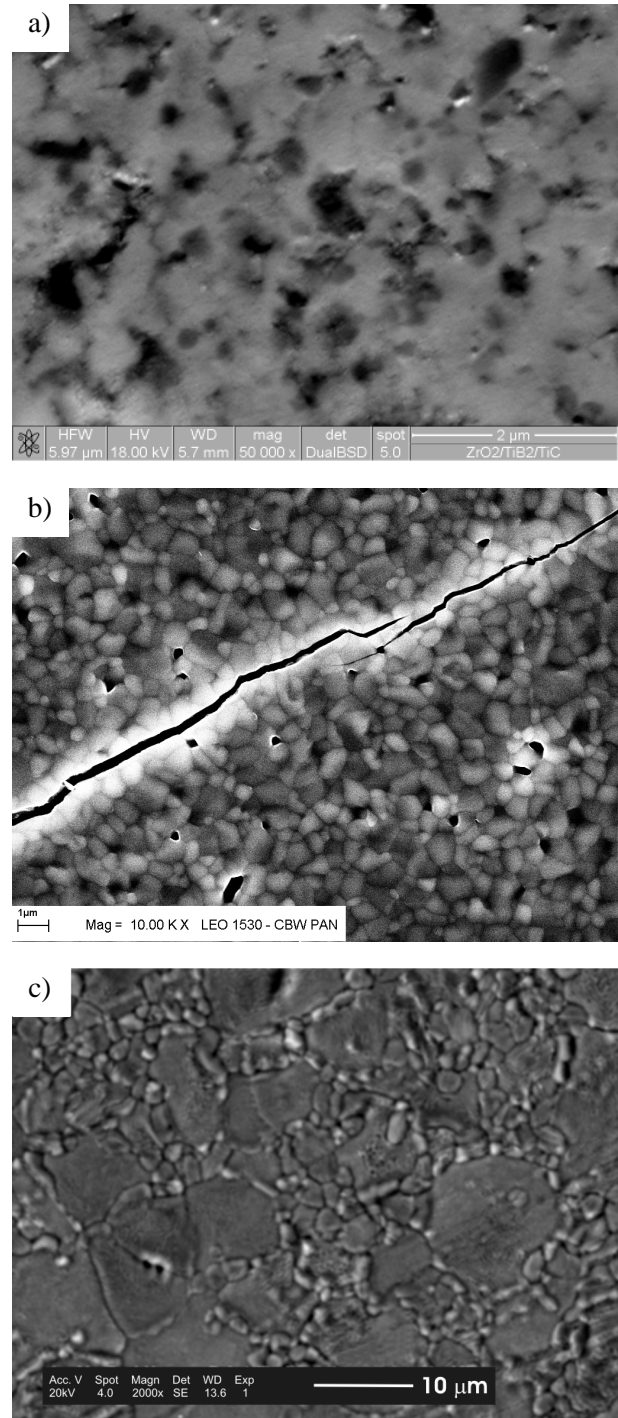


Fig. 8. SEM microphotographs of the sintered bodies: a) composite material; dark areas contained more Ti than the light ones as indicated by the EDS analysis, b) thermally etched surface of the composite, c) original TZP material. The surfaces were thermally etched at 1250°C.

Significantly improved mechanical properties of the zirconia/in-situ  $\text{TiB}_2$  composite were observed (Table 3). An increase of the bending strength,  $K_{IC}$  and hardness by 186%, 96% and 11% was measured, respectively.

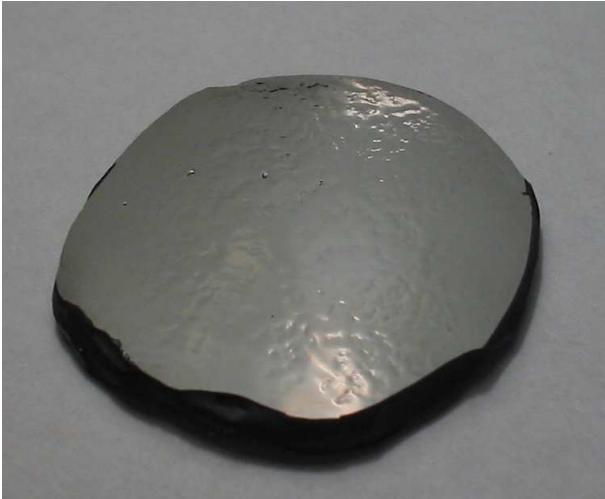


Fig. 9. Polished surface of the composite with surface pseudoplastic deformation due to the  $t \rightarrow m$  transformation

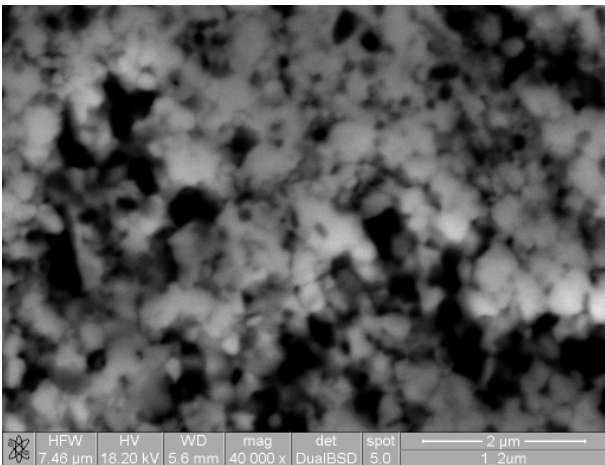


Fig. 10. Effects of the pseudoplastic deformation induced by  $t \rightarrow m$  transformation for the composite microstructure which occurred in a long period of time

The increased values of both bending strength and fracture toughness should be attributed to two factors. Firstly the composite microstructure was uniform and fine grained comparing to the original TZP which showed the symptoms of exaggerated grain growth. Secondly the tetragonal zirconia showed very high transformability to the monoclinic polymorph in case of the composite material as

indicated by the appearance of corrugated surface of the polished sample shown in Fig. 9. The effect looks like a pseudoplastic deformation and occurred shortly after cessation of polishing. This behaviour most probably resulted in compressive stresses in the surface layer of the material improving mechanical properties. However, destruction of whole material walking from the surface to the bulk occurred in a long period of time as shown in Fig. 10.

The crack deflection and crack bridging mechanisms of fracture toughness improvement were not found in the composite with in-situ synthesized inclusions (Fig. 8b). Crack propagated through the grains inducing very limited deflection and microcracking.

A hardness increase of the composite when compared to the original TZP of  $\sim 11\%$  is smaller than a value of 25% predicted by the rule of mixture. The rich in monoclinic phase microstructure and therefore susceptible to cracking is responsible for that result.

#### 4 Conclusions

The in-situ method is suitable for production of fine composite zirconia powders containing  $\text{TiB}_2$  and  $\text{TiC}$  microparticles. Consolidation of the composite powder by using hot pressing leads to production of the  $\text{TiB}_2/\text{TiC}/\text{ZrO}_2$  composite with improved mechanical properties. The composite derived from the 1.5 mol.%  $\text{Y}_2\text{O}_3$ -18 mol.%  $\text{TiO}_2$ - $\text{ZrO}_2$  nanopowder showed a bending strength of  $912 \pm 72$  MPa, a fracture toughness of  $8.8 \pm 0.5$   $\text{MPa} \cdot \text{m}^{1/2}$  and a Vickers hardness of  $12.2 \pm 0.2$  GPa. It seems that the optimised in-situ method has a production potential for  $\text{TiB}_2$  nanoparticles.

#### Acknowledgements

Financial support from the resources allocated for science in 2006-2008 under a research grant No. N507 017 31/0527 has been provided for this research work.

#### References

- [1] Vleugels J. and Van Der Biest O. "ZrO<sub>2</sub>-TiX Composites". *Key Engineering Materials*, Vol. 132-136, pp 2064-2067, 1997.
- [2] Vleugels J. and Van Der Biest O. "Development and Characterization of Y<sub>2</sub>O<sub>3</sub>-Stabilized ZrO<sub>2</sub> (Y-TZP) Composites with TiB<sub>2</sub>, TiN, TiC, and TiC<sub>0.5</sub>N<sub>0.5</sub>". *J. Am. Ceram. Soc.*, Vol. 82, No. 10, pp 2717-2720, 1999.
- [3] Basu B., Vleugels J. and Van Der Biest O. "Toughness Optimisation of ZrO<sub>2</sub>-TiB<sub>2</sub> Composites". *Key Engineering Materials*, Vol. 206-213, pp 1177-1180, 2002.

- [4] Rietveld H.M. Acta Cryst. 1967, 22, 151; Rietveld H. M., *J. Appl. Cryst.* Vol. 2, 65, 1969.
- [5] Rasband W., National Institutes of Health, USA, <http://rsb.info.nih.gov/ij/>
- [6] Niihara K.A. "A Fracture Mechanics Analysis of Indentation-Induced Palmqvist Crack in Ceramics". *J. Mater. Sci. Lett.* Vol. 2, pp 221-223, 1983.
- [7] Knacke O., Kubaschewski O. and Hesselmann K. (Eds.). "Thermochemical Properties of Inorganic Substances", 2 nd edition, Springer - Verlag Berlin, Heilderberg, 1991.
- [8] Allemann J.A., Michel B., Märki H.-B., Gauckler, L.J. and Moser, E.M. "Grain Growth of Differently Doped Zirconia". *J. E. Ceram. Soc.* Vol. 15, pp 951-958, 1995.
- [9] Pyda W. Microstructure and Properties of Zirconia-based Nanocomposites Derived from a Powder Containing TiC Crystallised *In-Situ* and Carbon". *Ceramics Int.* 30, Vol. 3, pp 333-342, 2004.
- [10] Hannink R.H.J., Kelly P.M. and Muddle B.C. "Transformation Toughening in Zirconia-Containing Ceramics". *J. Am. Ceram. Soc.* Vol. 83, pp 461-487 2000.
- [11] Pyda W. and Haberko K. "CaO-Containing Tetragonal ZrO<sub>2</sub> Polycrystals (Ca-TZP)". *Ceramics. Int.*, Vol. 13, pp 113-118, 1987.